OXFORD

Achieving symptom relief in patients with myalgic encephalomyelitis by targeting the neuro-immune interface and optimizing disease tolerance

Lucie Rodriguez (iD) [1], Christian Pou[1,†], Tadepally Lakshmikanth[1,†], Jingdian Zhang (iD) [2,3], Constantin Habimana Mugabo[1], Jun Wang[1], Jaromir Mikes[1], Axel Olin[1], Yang Chen (iD) [1], Joanna Rorbach (iD) [2,3], Jan-Erik Juto[4], Tie Qiang Li[4,5], Per Julin[6,7], Petter Brodin (iD) [1,8,*]

[1]Department of Women's and Children's Health, Karolinska Institutet, Solna 17121, Sweden
[2]Department of Medical Biochemistry and Biophysics, Karolinska Institutet, Solna 17176, Sweden
[3]Max Planck Institute Biology of Ageing—Karolinska Institutet Laboratory, Karolinska Institutet, Solna 17176, Sweden
[4]Department of Clinical Sciences, Intervention and Technology, Karolinska Institutet, Solna 17177, Sweden
[5]Department of Medical Radiation Physics and Nuclear Medicine, Karolinska University Hospital, Solna 17176, Sweden
[6]Department of Neurobiology, Care Sciences and Society, Karolinska Institutet, Solna 17176, Sweden
[7]Neurological Rehabilitation Clinic, Stora Sköndal, Sköndal 12864, Sweden
[8]Department of Immunology and Inflammation, Imperial College London, London W12 0NN, UK

*Correspondence address. E-mail: petter.brodin@ki.se
†These authors contributed equally to this work.

Abstract

Myalgic encephalomyelitis (ME) previously also known as chronic fatigue syndrome is a heterogeneous, debilitating syndrome of un-known etiology responsible for long-lasting disability in millions of patients worldwide. The most well-known symptom of ME is post-exertional malaise, but many patients also experience autonomic dysregulation, cranial nerve dysfunction and signs of immune system activation. Many patients also report a sudden onset of disease following an infection. The brainstem is a suspected focal point in ME pathogenesis and patients with structural impairment to the brainstem often show ME-like symptoms. The brainstem is also where the vagus nerve originates, a critical neuro-immune interface and mediator of the inflammatory reflex which regulate systemic inflammation. Here, we report the results of a randomized, placebo-controlled trial using intranasal mechanical stimulation targeting nerve endings in the nasal cavity, likely from the trigeminal nerve, possibly activating additional centers in the brainstem of ME patients and correlating with a ~30% reduction in overall symptom scores after 8 weeks of treatment. By performing longitudinal, systems-level monitoring of the blood immune system in these patients, we uncover signs of chronic immune activation in ME, as well as immunological correlates of improvement that center around gut-homing immune cells and reduced inflammation. The mechanisms of symptom relief remain to be determined, but transcriptional analyses suggest an upregulation of disease tolerance mechanisms. We believe that these results are suggestive of ME as a condition explained by a maladaptive disease tolerance response following infection.

Keywords: myalgic encephalomyelitis; systems immunology; disease tolerance; neuroimmunology

Introduction

According to recent estimates, myalgic encephalomyelitis (ME) affects as many as 2.5 million people in the USA alone [1]. The pathogenesis of ME remains poorly understood and no effective treatment is available for most of these patients. At last, the most recent few years have seen an increased activity in ME research, and the Institute of Medicine has recognized the condition in its recent report as a 'serious, chronic, complex system disease', bringing much needed legitimacy to patients facing skepticism and questioning from health care providers [2]. It is now clear that ME has a biological basis, but the disease is highly heterogeneous with variable severity and duration making it challenging to study. One of the most notable characteristic features of ME is the post-exertional malaise leading to significant deterioration of symptoms upon mental or physical activity over an individual threshold that is often quite low [3]. An immune system involvement is commonly seen, and many patients present with ME following an acute infection or virus reactivation, and multiple studies have reported elevated markers of inflammation in ME patients [4]. Some cytokines correlate with disease severity and a recent large study of nearly 200 ME patients found differences in T-cell subset composition and function when compared with healthy individuals [5, 6]. Our ability to profile human immune systems has improved with the advent of high-dimensional analysis methods such as mass cytometry, high-dimensional plasma proteomics and single-cell genomics [7–9]. Such methods now allow for all immune cells and many proteins and genes to be captured simultaneously and co-regulated features described [10]. Such systems immunology studies in healthy individuals have revealed that human immune systems are incredibly variable among individuals, but very stable within individuals over time, and most of this variation is attributed to non-heritable factors [11, 12]. Systems-level analyses also provide increased

resolution to detect differences in cell, protein and gene combinations associated with disease [13]. This becomes apparent when performing longitudinal profiling by systems-level immunomonitoring as perturbations associated with a disease process or response to therapy become apparent, and often such patterns would not be visible from reductionist analyses of individual immune system components alone [14–16].

Another clinical feature of ME is autonomic dysregulation, i.e. dysautonomia, with impairments to blood pressure regulation, temperature regulation, intestinal function and a range of other core physiological functions. Given the concomitant immune and autonomic perturbations in ME, it is conceivable that a common culprit could involve neuro-immune interfaces. The most studied such interface is the inflammatory reflex, a well-known anti-inflammatory reflex mediated by the vagus nerve [17]. Direct infection of vagus nerve fibers has been suggested as a possible pathogenic mechanism in ME and some patients with cervical compression and impaired circulation of cerebrospinal fluid can present with ME-like symptoms, which sometimes are reversible upon decompressive surgery [18, 19]. Moreover, afferent fibers in the vagus nerve can sense microbial stimuli and dysbiosis in the gut and elsewhere that can fuel chronic inflammation in ME [20].

Several treatment modalities target the vagus nerve; implanted electrical nerve stimulators in patients with severe epilepsy, as well as non-invasive stimulators using mechanical stimulation of mechano-sensitive nerve endings in the ear, or on the neck, can stimulate the vagus nerve nuclei in the brainstem and trigger the inflammatory reflex [21, 22]. As an alternative treatment modality, intranasal mechanical stimulation (INMEST) and the related kinetic oscillatory treatment (KOS) use mechano-stimulation to trigger nerve endings in the nasal cavity, likely belonging to the trigeminal nerve and propagating signals to the brainstem where they could potentially impact vagal tone [23, 24]. Curiously, the use of such treatments in patients with acute migraine and chronic inflammatory disorders has correlated with reduced markers of systemic inflammation [25, 26]. Functional MRI in healthy volunteers treated with INMEST shows increased activity in the vagus nerve nuclei, but the effects on heart-rate variability, a complex measurement of autonomic regulation and the balance between sympathetic and parasympathetic tone, differs between these vagus stimulating treatment modalities [23, 24, 27]. Other studies describe non-invasive vagus nerve stimulation (nVNS) with KOS as targeting vagal afferents in the context of observing the modulation of the cranial trigeminal autonomic reflex [28].

Here, we reasoned using INMEST in patients with ME to alter the neuro-immune interface as seen in patients with other inflammatory disorders [26]. Combined with longitudinal systems-level immunomonitoring, our hope was to analyze such perturbations to better understand immunological processes underlying ME and correlate these with possible treatment responses. We performed a placebo-controlled, double-blinded, randomized trial of INMEST given biweekly for 8 weeks. The clinical improvement was significantly better with active INMEST than with placebo and represented ~30% reduction in symptom intensity after 8 weeks. We also found measurable changes in immune measurements that suggest perturbations involving IL-17-mediated inflammation, immune cell energy metabolism and a failure to induce disease tolerance as elements of ME pathogenesis. These results suggest novel lines of mechanistic investigation into disease and that INMEST is a simple and safe method for symptom relief through a re-calibration of the neuro-immune setpoint.

Results
ME symptom relief after INMEST treatment
We enrolled 31 patients with moderate-to-severe ME (17 in 2018 and 14 in 2019). All of these fulfilled the Canadian consensus criteria. These subjects were randomized to one of two arms within a double-blinded, randomized control trial to receive 20 min of INMEST twice a week for 1 month, or placebo treatment, which is indistinguishable from active INMEST to the patient and the treating physician. This point is important to avoid bias from changes to the patient–doctor relationship. Previous studies of KOS treatment have demonstrated the indistinguishable sensation between active and placebo treatment [28]. Following the first month of placebo or active treatment, all subjects were exposed to active INMEST treatment 20 min bi-weekly (Fig. 1A). The INMEST device consists of a thin plastic probe placed in the nose that vibrates at a set frequency to mimic turbulent airflow within the nasal cavity and induces a nerve reflex, likely mediated via the trigeminal nerve and transmitted to brainstem with possible effects on the vagus nerve [24] (Fig. 1B). It is important to note that possible effects of INMEST on the vagus nerve are not fully understood and only supported by preliminary data so far. It is seemingly different from classic vagus nerve stimulation as used in patients with epilepsy and likely multifactorial requiring further mechanistic investigation in the future. INMEST has been shown to alter the balance between sympathetic and parasympathetic tone, resulting in a reduction of heart-rate variability [23].

Our current study is not powered to test the possible beneficial effects of the INMEST treatment on patient outcome. Instead, the purpose of the INMEST treatment here is to induce a possible perturbation to the immune system, that in combination with systems-level monitoring allows us to decipher possible mechanisms of immune system activation in ME patients (Fig. 1C). This method of system-wide perturbation and longitudinal monitoring is a common method in systems biology to better understand regulatory mechanisms in physiological systems [29].

The primary outcome measure in this study was fatigue as defined by the fatigue severity scale (FSS), but no significant effect of INMEST treatment was seen for this outcome variable [30]. We also evaluated overall symptom scores using a questionnaire previously shown to distinguish subgroups of ME patients [31]. During the first month of treatment, the placebo showed a modest response of ~10% reduction in symptom score, while the actively treated patients initially improved, then displayed a rebound effect, followed by a more significant improvement and a total ~20% overall reduction in symptom scores after the first 4 weeks (8 active treatments) (Fig. 1D). It is important to note that many patients struggled with biweekly visits to the clinic and some patients suffered episodes of deterioration as a consequence of post-exertional malaise. During the second phase of active INMEST treatment (for all patients), symptom scores decreased further and in patients receiving active treatment only ~30% decrease in symptom scores were achieved at the end of the 8-week trial (16 active treatments) (Fig. 1D). Since treatments varied slightly over different days, but result was the same if plotted against the number of treatments rather than days of study (Fig. 1D). The effect was significantly stronger ($P = 0.00003$) in the patients receiving active treatment only versus patients receiving placebo followed by active treatment (Fig. 1D), and the response persisted after cessation of treatment in both groups and even improved further in the most actively treated group, suggesting that further improvements could be possible with a prolonged treatment protocol (Fig. 1D).
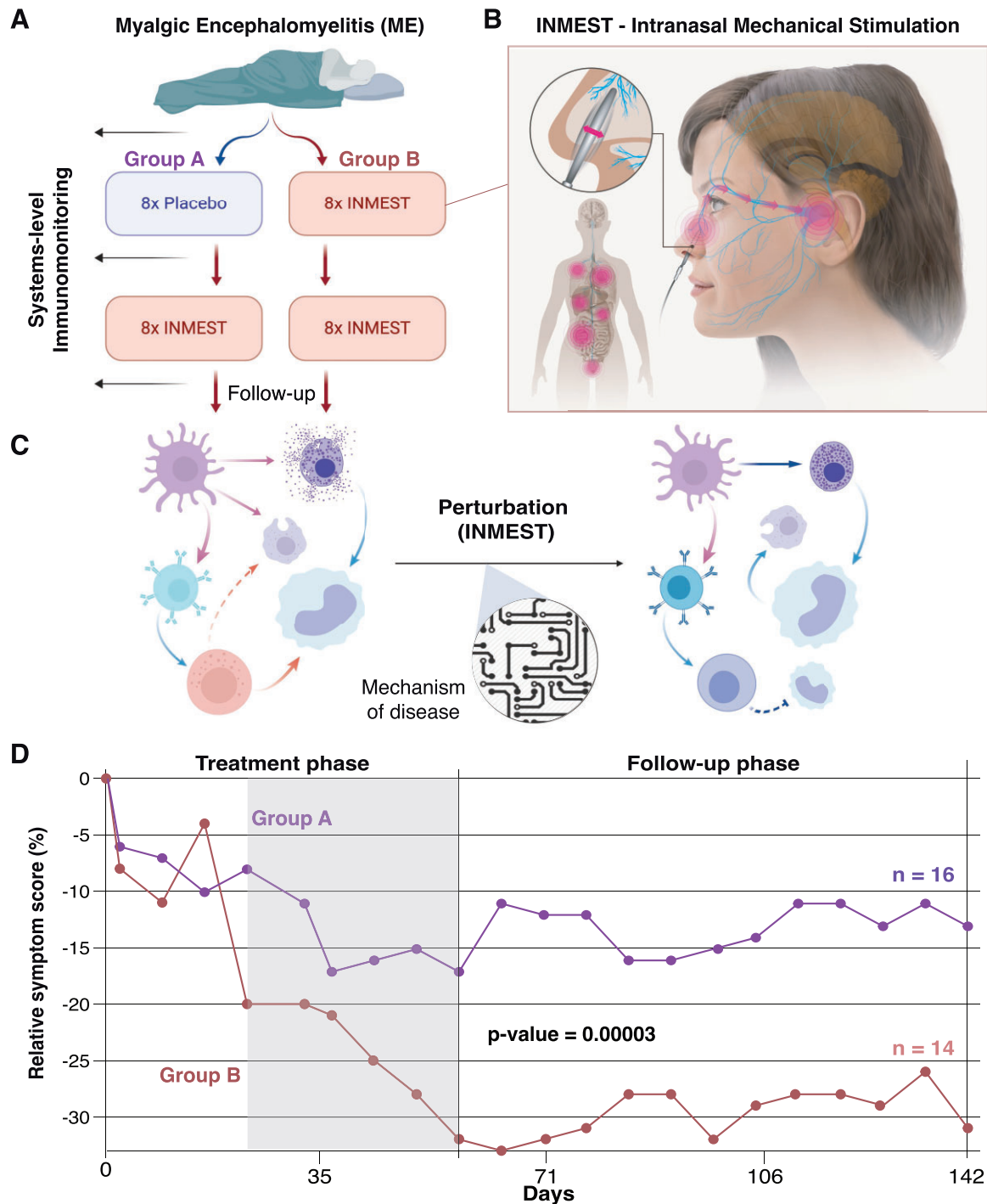
Figure 1. Study design, treatment and outcome. (**A**) Study design and sample collection for systems-level immunomonitoring. (**B**) INMEST. (**C**) Treatment (INMEST) is used as a perturbation to probe mechanisms of disease in ME patietns. (**D**) Change in symptom score (rating scale of symptom severity from the ICC criteria to evaluate disease burden) in patients randomized to Group A ($n = 16$) versus Group B ($n = 14$). Y-axis indicate average ME symptom scores relative to baseline (average for each patient group at different timepoints (tpt)—ME symptom score at tpt/baseline ME symptom score). Treatment phase includes weekly samples as the placebo/INMEST treatment was given bi-weekly after baseline sample collected, first phase includes Group A—4× Placebo and Group B—4× INMEST treatment and in second phase both groups received 4× INMEST treatment (highlighted in grey) before follow-up phase (post-INMEST). Patients receiving only active treatment (Group B) showed a significantly stronger effect and decrease in symptom score ($P = 0.00003$) versus patients receiving placebo followed by active treatment (Group A).

Immune system measurements correlate with symptom relief

To understand the underlying immune system perturbation in ME, and investigate any potential changes correlating with treatment response, we collected blood samples at baseline before treatment, after phase 1 (4 weeks), and after phase 2 (8 weeks) (Fig. 2A). To minimize technical variation, samples were prepared directly at blood draw and cells frozen in whole blood stabilizer solution, plasma centrifuged and frozen, and whole blood bulk mRNA stabilized and frozen [32, 29] (Fig. 2A). We performed
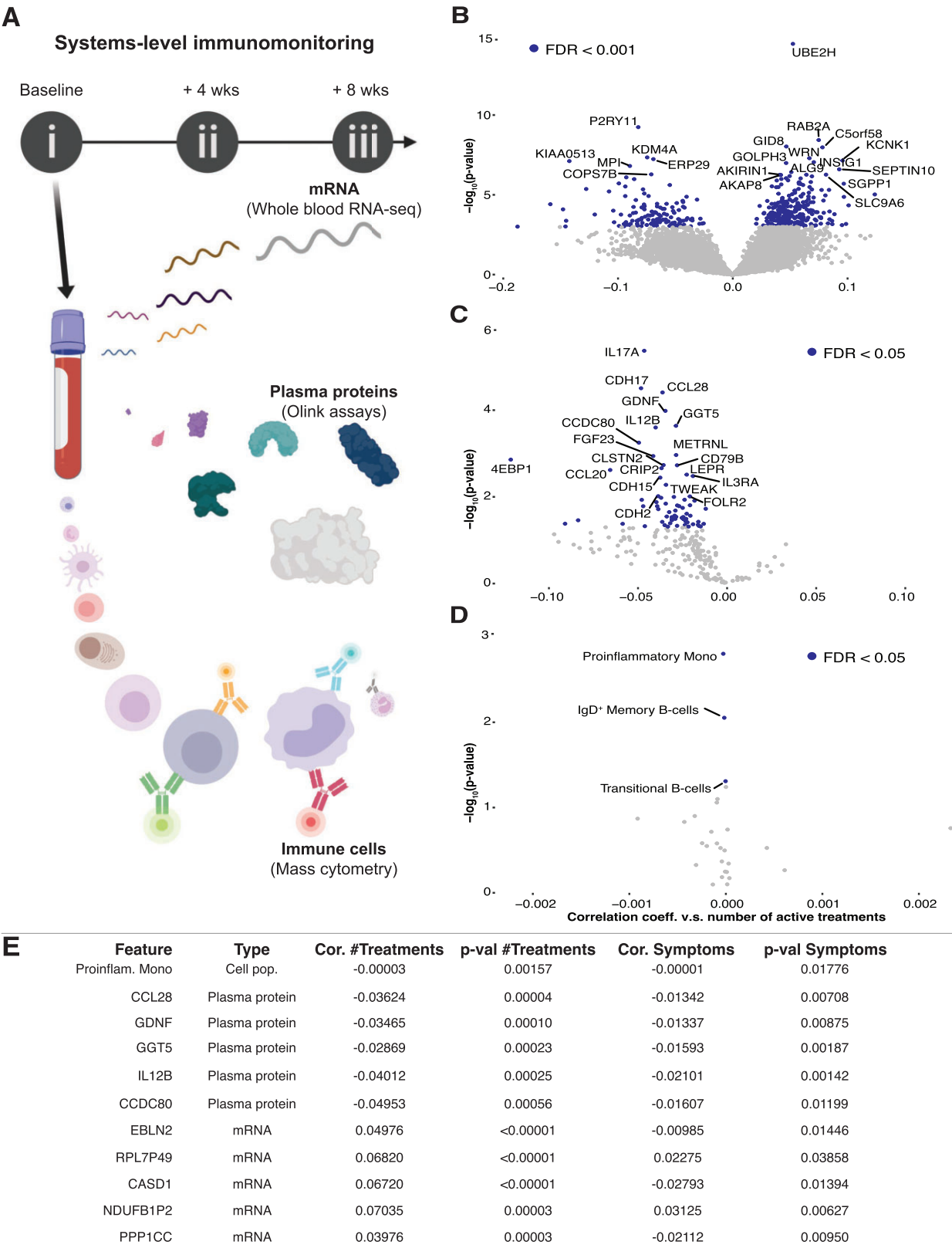
E

Feature	Type	Cor. #Treatments	p-val #Treatments	Cor. Symptoms	p-val Symptoms
Proinflam. Mono	Cell pop.	-0.00003	0.00157	-0.00001	0.01776
CCL28	Plasma protein	-0.03624	0.00004	-0.01342	0.00708
GDNF	Plasma protein	-0.03465	0.00010	-0.01337	0.00875
GGT5	Plasma protein	-0.02869	0.00023	-0.01593	0.00187
IL12B	Plasma protein	-0.04012	0.00025	-0.02101	0.00142
CCDC80	Plasma protein	-0.04953	0.00056	-0.01607	0.01199
EBLN2	mRNA	0.04976	<0.00001	-0.00985	0.01446
RPL7P49	mRNA	0.06820	<0.00001	0.02275	0.03858
CASD1	mRNA	0.06720	<0.00001	-0.02793	0.01394
NDUFB1P2	mRNA	0.07035	0.00003	0.03125	0.00627
PPP1CC	mRNA	0.03976	0.00003	-0.02112	0.00950

Figure 2. Systems-level profiling reveals immune perturbations. (**A**) Blood samples were collected and immediately processed for whole blood mRNA-seq (PaxGene tubes), mass cytometry (stabilized whole blood cells) and plasma proteins (immediate centrifugation) by Olink assays. (**B–D**) Volcano plots of differentially regulated features versus number of active treatments. (**E**) Mixed-effects modeling shows the most perturbed plasma proteins and immune cells that change in response to therapy and in relation to symptom scores.

immune cell compositional and phenotypic analysis using mass cytometry; plasma protein analysis by Olink assays and whole blood mRNA-sequencing to gather different perspectives of the global immune state in ME patients before, during and after treatment time. The gene most significantly induced by active INMEST treatment was the E2 ubiquitin-conjugating enzyme

UBE2H (Fig. 2B), a gene broadly expressed by blood immune cells (https://www.proteinatlas.org/ENSG00000186591-UBE2H/blood) that stimulates ubiquitin-mediated degradation of dysfunctional proteins. Plasma cytokines IL-17A, IL-12B and CCL28 were among the top plasma proteins decreasing after INMEST treatment (Fig. 2C) and these have all been previously reported to be involved in ME [32]. Circulating immune cells also changed, especially the proinflammatory monocytes that decrease over time during INMEST treatment (Fig. 2D).

Next, we used mixed-effects modeling to test whether individual immune system measurements were associated with symptom relief as measured by symptom score questionnaires. We also used age, sex, treatment group (pre-/post-INMEST) and number of treatments as fixed effects and found that frequencies of proinflammatory monocyte in the blood, plasma IL-12B and CCL28 and other pro-inflammatory mediators decreased as symptom scores decreased after INMEST treatment [1] (Fig. 2E). These results further underscore the inflammatory nature of ME with observable variable levels of cytokine elevation in plasma that correlate with symptom severity. Our results also show that the biomarker correlates of response in ME patients could be measured in the blood.

Multi-omics factor analysis reveals co-regulated biomarkers in ME

Immune cells and proteins do not function in isolation but coordinate their actions into a complex network of communicating features. Multi-omics factor analysis (MOFA) is a method for integrating different types of data and allow such coordinated features to be identified and associated with a condition of interest in the form of latent variables that discriminate groups of samples [32]. MOFA was applied in our cohort to all plasma proteins, immune cell frequency and mRNA measurements across all blood samples ($n=85$). A range of variable MOFA models were run with different constraints until a model with 10 latent factors (LFs) was found to explain the variance among the samples (Fig. 3A and B). We inspected samples across these LFs to identify any factor that could segregate samples collected before and after INMEST treatment. LF7 showed such a gradient from pre- to post-INMEST samples and we focused on this LF (Fig. 3C). In LF7, 65% of genes and 50% of plasma proteins overlapped with the significant features in the mixed-effect model above, emphasizing that features associated with INMEST response can be measured in blood, but the MOFA result also broadens the scope of immunological features influenced by INMEST (Fig. 3D) [33].

Cell–cell relationships are perturbed in ME

Given the coordinated changes induced by INMEST treatment across different immune system components, we decided to take a closer look at cell–cell dependencies and how these would be rewired by treatment. This is important because all immune responses occur as concerted efforts by multiple cell populations, and perturbations to such relationships can be an element of disease [34]. To this end, we compared cell–cell correlation matrices before and after INMEST treatment and we found specific cell–cell relationships changing after INMEST treatment (Fig. 4). For example, positive associations were found between naïve and central memory T-cells, that became more pronounced after INMEST, likely reflecting an improved cell–cell coordination within the system as a consequence of dampened inflammation described above (Fig. 4B).

Moreover, a specific module of cells involved mucosal-associated invariant T-cells (MAIT cells) and marginal zone (IgD$^+$ memory) B-cells, both known to be important cells interacting with microbes in the gut [35]. MAIT cells have been implicated in ME previously [6, 19]. In these cell–cell correlation analyses, these effector cells correlated inversely with antigen-experienced (memory) regulatory T-cells, a type of cell known for its critical importance in maintaining homeostasis at barrier surfaces such as the gut [36]. This relationship was not visible at baseline (Fig. 4A), but appeared after INMEST treatment, indicating a normalization of a critical immune cell module and regulatory mechanism in parallel with symptom relief (Fig. 4B). We think this finding represents another clue into ME pathogenesis and the mechanism of action of INMEST, since gut microbial dysbiosis have been reported in ME [20]. The vagus nerve can convey afferent signals of gut dysbiosis to the brainstem and trigger immune regulation via the inflammatory reflex [30, 31]. The reduction in plasma IL-17A and CCL28 levels after INMEST and the restored MAIT/regulatory T-cell relationship indicates a modulation of this axis by INMEST treatment and mitigation of an inflammatory state originating at the immune microbe interface in the intestine. Also, the common Epstein–Barr virus often associated with ME has been reported to induce IL-17 and reactivation of this virus is another possible chronic immune stimulation in ME patients [37].

Transcriptional programs altered in ME patients treated by INMEST

To further investigate the possible mechanisms of action of INMEST in these ME patients, we investigated the whole blood transcriptome more in-depth. INMEST treatment upregulated 142 genes (P-value < 0.05) and downregulated 12 384 genes (P-value < 0.05), a gene set enrichment analysis (GSEA) was performed on these differentially regulated genes in order to understand the molecular pathways affected [38] (Fig. 5A). The most enriched Gene Ontologies (GOs) are shown in Fig. 5A and involve three broad biological processes: (i) nerve cell signal transmission, (ii) immune response pathways and (iii) cellular metabolism (Fig. 5A), all previously linked to the pathogenesis of ME [1].

A set of genes involved in 'long-term synaptic potentiation' increased mRNA expression with INMEST treatment, particularly after more than eight treatment sessions (Fig. 5B). Examples include SYNC, a gene encoding the protein alpha-synuclein present in neuronal presynaptic terminals and regulating neuronal signal transmission [39]. The T-cell co-stimulation gene set involves molecules such as CD86 on antigen-presenting cells, which are necessary for co-stimulating T-cells activated by antigens. Most of these genes' expression decreased after INMEST in line with an overall dampening of immune cell activation in ME patients treated with INMEST (Fig. 5C).

In a recent study by Davis and colleagues, blood cells from ME patients were reported to display a unique impedance pattern in response to hyperosmotic stress suggesting that a nano-electronic impedance sensor could be used in a diagnostic test for ME [40]. We find that the GO: 'Response to osmotic stress' was associated with INMEST treatment and genes involved include the Bcl2 family member BAX, which decreased in mRNA expression upon treatment (Fig. 5D).

Finally, multiple gene sets regulated by INMEST involved cellular energy metabolism, which is curious given that fatigue is the cardinal symptom of ME and linked to alterations in cellular metabolism [41]. 'The GO: Negative regulation of cellular carbohydrate metabolism' is affected by INMEST with genes like GCK encoding the glucose sensor glucokinase, which shifts cellular
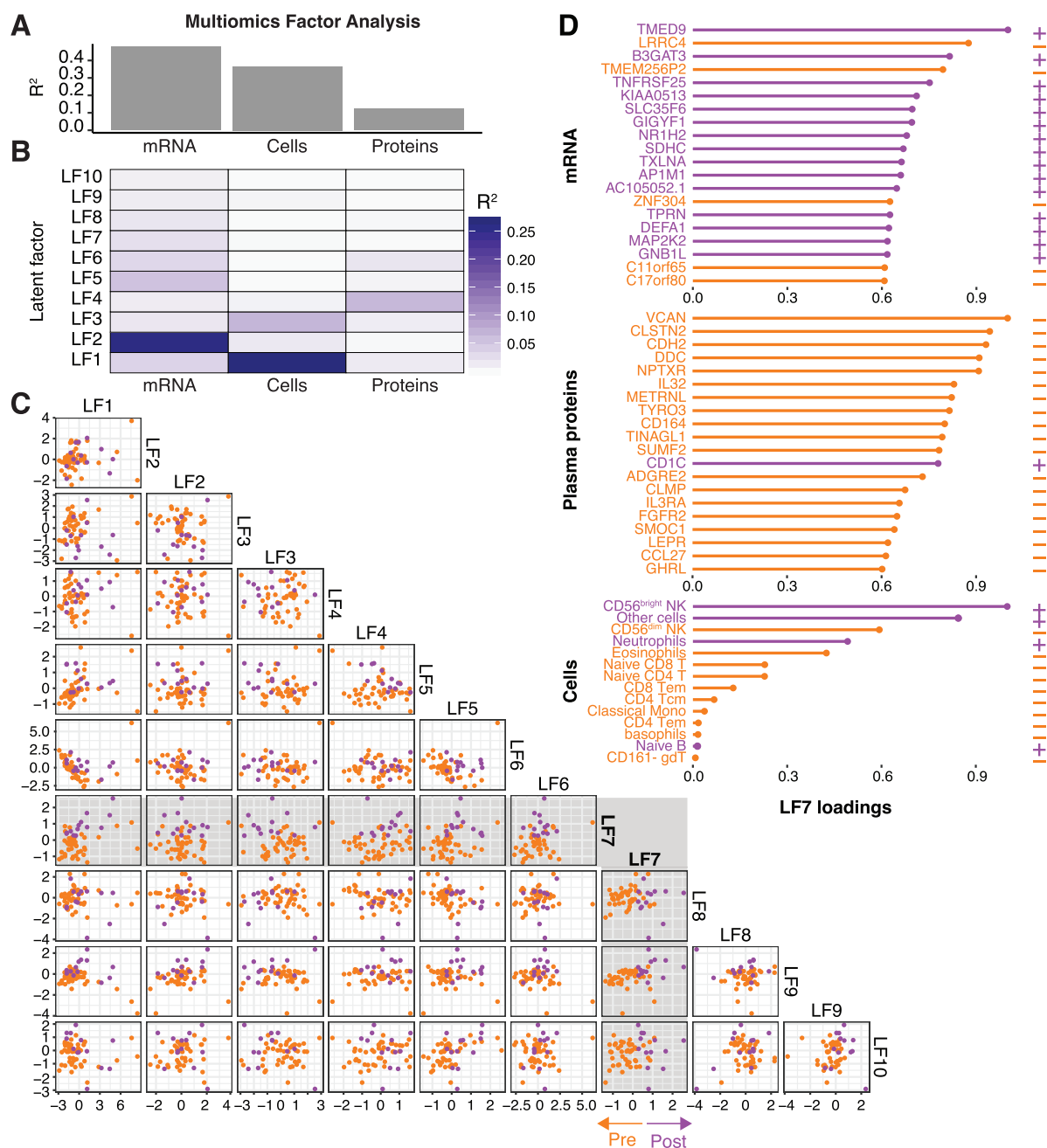
Figure 3. Co-regulated immune features revealed by multi-omics factor analyses. (**A**) Variance explained by different views (immune cells, proteins and mRNA). (**B**) Variance explained by each of the calculated LFs. (**C**) Scatterplot showing individual samples and their LF distributions. (**D**) Top features contributing to LF7 associated with INMEST treatment response.

metabolism based on the availability of glucose and was found in this cohort to be repressed in ME patients after INMEST treatment [42] (Fig. 5E).

To investigate changes in energy metabolism in ME patients, we took advantage of the Agilent Seahorse analysis of energy metabolism using cultured PBMCs collected from ME patients at baseline, and after 8 and 16 treatment rounds (Fig. 5F). This assay measures the multiple aspects of cellular metabolism and ATP usage and oxidative phosphorylation. As predicted by mRNA-sequencing results above, we find improvements in energy metabolism in cultured PBMCs from ME patients treated with INMEST. This improvement involved both maximal respiration (Fig. 5F) and spare respiratory capacity (Fig. 5G), suggesting that INMEST impacts OXPHOS pathways reported to be

perturbed in ME patients in some, but not all prior studies performed [43].

ME—a failure of inducing disease tolerance upon chronic immune activation

Given the evidence of chronic immune activation in ME and the multifaceted symptoms in ME, we considered possible unifying mechanisms that could explain the variable presentation of this mysterious illness. Disease tolerance is an overall term describing a range of stress–response pathways that limit tissue damage caused by invading pathogens or indirectly by host immune responses [44]. We hypothesized that ME could be due to a failure of upregulating such disease tolerance mechanisms in response to infection. To this end, we analyzed genes involved in disease
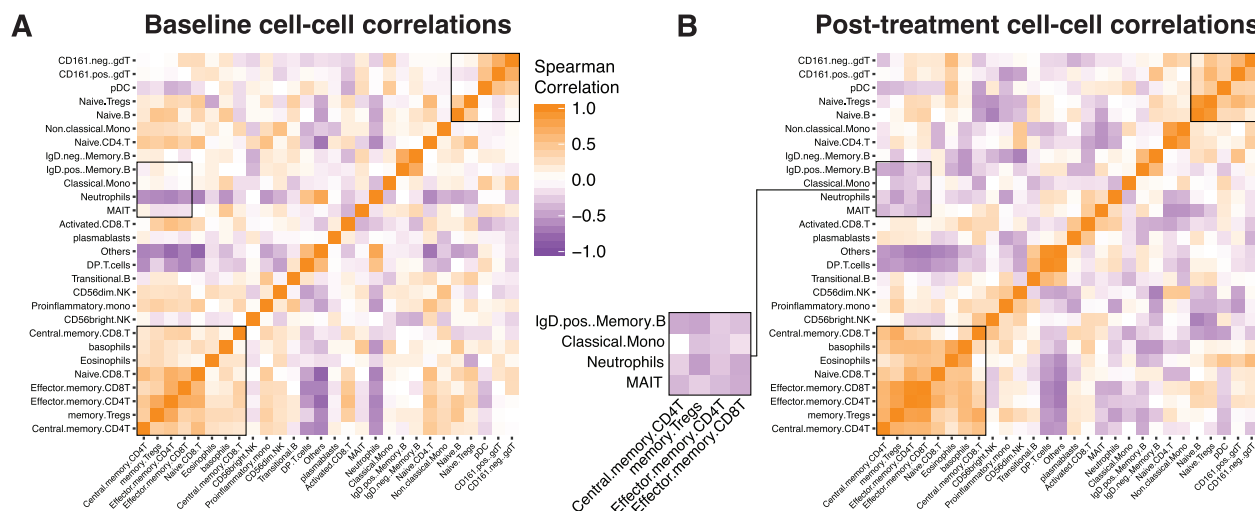
Figure 4. Immune cell function in ME patients treated with INMEST. (**A**) Spearman correlation matrix showing co-regulated cell population frequencies at baseline and (**B**) after 16 active INMEST treatments, indicating re-establishment of specific cell–cell relationships, such as the highlighted module involving MAIT cells and marginal zone B-cells (IgD+ mem. B) negatively correlated with memory Tregs.

tolerance induction based on a transcriptional regulatory network database TRRUST v2 [45]. Most effector genes increased their mRNA expression after active INMEST treatments in ME patients (Fig. 6A–C), supporting the hypothesis that induction of disease tolerance could mitigate ME symptoms. We then focused on disease tolerance pathways most strongly upregulated with treatment. HIF-regulated effector genes like VEGFA, CXCR4, AR and SERPINE1 are induced by tissue hypoxia during infections, a response important for limiting tissue damage potentiated by INMEST treatment (Fig. 6A–C). Saha *et al.* [46] have reported higher levels of reactive oxygen species (ROS) in red blood cells of ME patients compared with healthy controls, and up-regulation of the oxidative stress response pathway upon INMEST (SIRT1) corroborates this observation. These upregulated pathways and the induction of genes in the insulin receptor signaling pathway, heat shock proteins and cell cycle regulators all support the idea that INMEST treatment upregulates disease tolerance pathways normally induced during infections, and possibly improperly suppressed in ME patients (Fig. 6A–C). In conclusion, our findings show evidence of chronic immune activation in patients with ME, particularly involving the IL-17 pathway, MAIT cells and other intestinal lymphocytes interacting with microbes. The INMEST treatment induces a significant symptom relief that correlates with a normalization of immune cell regulatory networks, cellular metabolism and upregulation of disease tolerance programs.

Discussion

Our findings paint a picture of ME as a truly multifaceted disorder involving inflammation with a possible origin at the immune–microbe interface in the gut. Chronic immune stimulation is likely given the symptomatology, but also elevated cytokine levels are found that correlate with symptom severity and immune cell deficiencies [5, 6]. The deficiencies in cellular metabolism are not typically seen in other inflammatory diseases, although transient metabolic adaptations are common during acute immune responses [47].

It is important to note that ME is a heterogeneous disease and the likelihood of finding one pathogenic mechanism shared by all patients is low. We believe that one unifying concept could be the failure in upregulating disease tolerance mechanisms in the

event of an infection or virus reactivation and this is what we propose herein. Such disease tolerance mechanisms are important in limiting the reduction in host fitness as a consequence of the infection directly or as a consequence of the elicited immune defenses [44]. Our data of upregulated disease tolerance pathways upon INMEST treatment support the hypothesis that ME is caused by maladaptive physiological response to an infection and failure of inducing disease tolerance leading to deterioration of physiological functions (Fig. 6D). This physiological maladaptation to infection is supported by abnormally low levels of hypothalamus–pituitary–axis hormones in patients with ME [48].

The reasons why ME patients differ so much in their symptomatology could be explained by differences in the underlying infectious disease or immune activation, and the relevant disease tolerance pathway failing to be induced. The reasons for why ME patients would fail to upregulate disease tolerance pathways remain to be determined, although one interesting lead comes from an observation made of mutations in the enzyme IDO2 seen in 20/20 patients with severe ME (https://www.omf.ngo/2018/10/19/healthrising-the-metabolic-trap-shines-during-the-symposium-on-the-molecular-basis-of-me-cfs-at-stanford/) and has led to the formulation of the metabolic trap hypothesis of ME [49]. However, the IDO enzymes are also involved in disease tolerance, specifically upon exposure to endotoxin, a component of Gram-negative bacteria in the gut [50, 51].

The symptom relief induced by INMEST was significant and distinct from placebo, but still must be confirmed in larger trials with sufficient statistical power. We believe that this should be done using a self-treatment system available for use at home since the repeated visits to the clinic are difficult for patients with ME and might worsen symptoms. The main purpose of the current study was instead to use the INMEST treatment as a perturbation to the immune system and autonomic inflammatory reflex, as a means of uncovering the pathogenesis of the disorder. To this end, the current study was successful and the biomolecular correlates found corroborate several previously suggested aspects of ME pathogenesis.

The mechanism of action of the INMEST treatment in ME is not known. Preliminary data, not yet peer reviewed, but reported at a conference, suggest that the vagal motor nuclei in the brainstem was activated by INMEST, but also higher level centers such
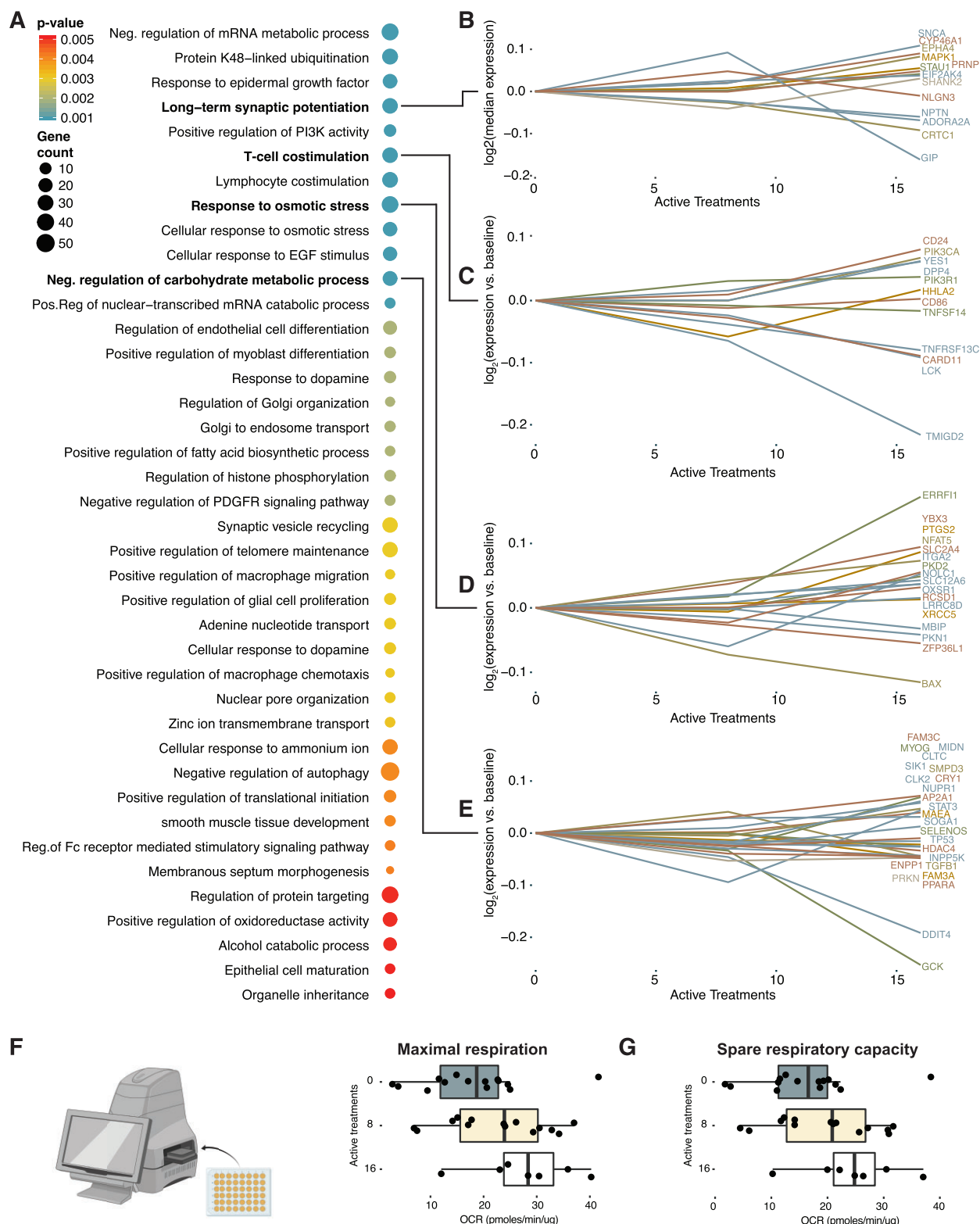
Figure 5. Immune cell metabolism is impaired in ME but normalized by INMEST. (**A**) GSEA for genes differentially regulated in response to INMEST treatment. (**B–E**) Four highlighted GO terms and the top genes with the largest absolute change in response to INMEST treatment. (**F**) Maximal respiration in cultured PBMC from ME/CFS patients at baseline, and upon 8 and 16 active INMEST treatment rounds, respectively ($n = 13$). (**G**) Spare respiratory capacity (SRC) in cultured PBMC from ME/CFS patients at baseline, and upon 8 and 16 active INMEST treatment rounds, respectively ($n = 13$).

as the limbic system was activated [24]. Given its placement in the nasal cavity, it is likely that nerve endings belonging to the trigeminal nerve are initially triggered by INMEST and convey signals to the brainstem. The relative contribution of this cranial

nerve and others like the vagus nerve is unknown and a lot more mechanistic investigation is required to fully understand the neurophysiological effects of the INMEST treatment but such investigations are beyond the scope of the current study. The
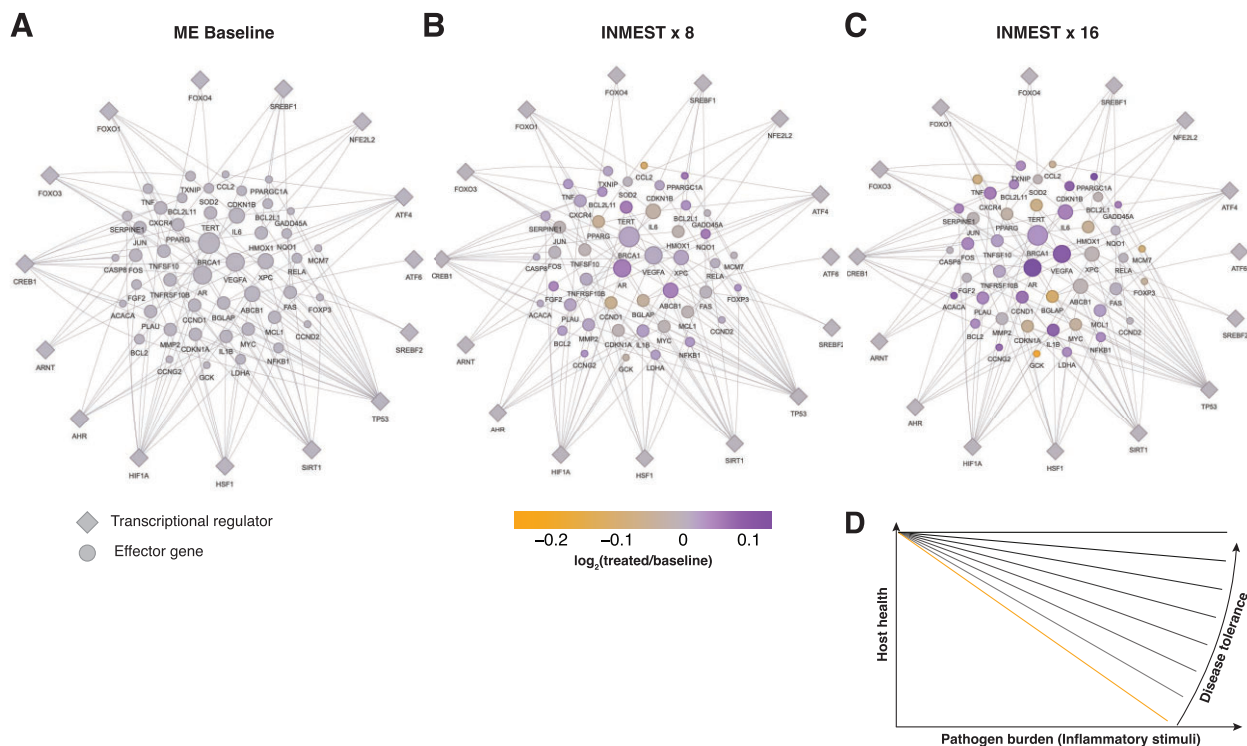
Figure 6. INMEST treatment induces disease tolerance programs in ME patients. Transcriptional regulators (diamonds) and their target genes involved in disease tolerance are shown in ME patients (**A**) at baseline and (**B**) after 8 and (**C**) 16 rounds of INMEST treatment. (**D**) A proposed model of ME as a disease caused by failure to upregulate disease tolerance mechanisms in response to chronic inflammatory stimulus leading to broad impairments and reductions in overall health. Size of the nodes refers to the number of regulatory interactions (larger = more regulatory interactions).

effect of INMEST on heart-rate variability differs from that of traditional vagus nerve stimulating methods [23]. One possibility is that INMEST influences incoming (afferent) signals from the gut, conveying signals of dysbiosis or chronic immune activation and inflammation. This hypothesis is in line with previous proposals of ME as a disease caused by microbial dysbiosis in the gut and symptom relief upon INMEST treatment could occur by limiting such signals of dysbiosis via the afferent vagus nerve [52].

A problem with the treatment trial presented here is that ME patients were required to visit the clinic twice weekly for 8 weeks in order to receive treatments and provide blood samples as well as respond to questionnaires. All of these activities were very demanding and caused deterioration in some patients that obscure some of the possible benefits of the therapy. We found no significant improvement of the primary outcome measurement, fatigue in this study. One possible explanation for this is the recurrent clinical visits and the consequent worsening of disease. Another possible explanation is related to the FSS, this questionnaire has been shown to best distinguish patients with ME from healthy individuals, while its ability to capture quantitative changes within patients over time is in question, and ceiling effects have been reported [53]. In the future, a more sustainable way of using INMEST would be in the form of a self-treatment device used by subjects and care takers at home. Obviously, larger follow-up studies are required to further assess the clinical value of this approach more generally in ME patients. It is likely important to improve the diagnostic accuracy of ME and ensure more homogenous group of patients included in order to sharpen our ability to understand the underlying pathology in ME, subdivide patient groups and test treatment strategies in these different subgroups accordingly. The recent advances in diagnostic tests are promising in this regard [40]. We hope that this work will

inspire others to further investigate the immune/microbe interface and the failure to induce disease tolerance in ME and hopefully this increased attention will lead to some further relief to the millions missing due to this devastating condition.

Materials and methods
Study design
The sample size was based on the patients who had volunteered to take part in the clinical trial up to the point we started analysis; therefore, both of the first two cohorts were included in the study. All samples were included in the trial unless the patients opted to drop-out of the clinical trial before the end of the study, solely on patient opted to drop-out of the clinical trial and was no included in the cohort. The Swedish ME cohort that underwent the INMEST treatment comprises of a gender-mixed group, 23 females and 8 males. Female patients had a median age of 42 (range: 19–62) and male patients had a median age of 35 (range: 26–66). All were evaluated for enlistment based on the Canadian consensus criteria [54]. The INMEST treatment for the clinical trial (NCT03502044) was undergone at the Neurological Rehabilitation Clinic in Stora Sköndal with Dr Per Julin as the lead investigator. The research group has used INMEST and KOS interchangeably until 2018, reason for the latter term being used on clinicaltrials.gov.

Experimental design
The randomized, placebo-controlled and double-blinded trial of INMEST included two weekly doses over the span of 8 weeks. The double-blinded trial was possible due to the INMEST device that consists of a thin plastic probe inserted in the nasal cavity and set to vibrate at a set frequency when active. These vibrations are

not perceived by the patients receiving active treatment as whether the device is active or inactive is indistinguishable by the patients or doctors. The doses included 10 min of placebo or active INMEST treatment in each nasal cavity (20 min total). For each cohort, the INMEST device randomly selected either placebo or active treatment during the first 4 weeks followed by only active treatments the following 4 weeks. During the first 4 weeks, both the patient and doctor were blind as to whether placebo or active treatment was given. In the end, the active–active group included 5 males and 11 females while the placebo–active group included 3 males and 12 females.

One of the key factors that was recorded during this study is the ME symptom rating scale, it is a rating scale of the severity of symptoms from the ICC criteria on a 5-degree scale from 0 to 4 (none, light, moderate, severe and very severe) in order to evaluate degree of disease burden in accordance to the Canadian Consensus criteria. Other than symptom severity, the following measures were recorded for the clinical trial: FSS, SF-36 Physical Functioning Subscale (PF-10), Hospital Anxiety Depression Scale, EQ5D, as well as Visual Analogue Scale (VAS). Blood samples were collected at 3 timepoints for each patient (baseline) and subsequentially at 8 treatments (T1—4 weeks) and 16 treatments timepoints (T2—8 weeks).

Immune cell phenotyping by mass cytometry

Cryopreserved and stabilized whole blood (blood mixed with 'stabilizer' component of whole blood processing kit; Cytodelics AB, Sweden) collected from ME patients sampled thrice [baseline, T1 (4 weeks) and T2 (8 weeks)] during the study period were thawed, and cells were fixed and RBCs lysed using lysis and wash buffers (Whole blood processing kit; Cytodelics AB) as per the manufacturer's recommendations. This was performed a few days prior to barcoding and staining of cells. Post fix/lysis of cells, $\sim 1 \times 10^6$ cells/sample were plated onto a 96-well 'U' bottom plate using standard cryoprotective solution [10% DMSO and 90% fetal bovine serum (FBS)] and cryopreserved at $-80°C$. On the day of barcoding and staining of cells, cells were thawed at 37°C using RPMI medium supplemented with 10% FBS, 1% penicillin–streptomycin and benzonase (Sigma-Aldrich, Sweden). Briefly, cells were barcoded using automated liquid handling robotic system (Agilent Technologies, Santa Clara, CA, USA) using the Cell-ID 20-plex Barcoding kit (Fluidigm Inc.) as per the manufacturer's recommendations [41]. Following cell pooling batch-wise (with samples from placebo and treatment groups equally represented in each batch), cells were washed, FcR blocked using blocking buffer (in-house developed recipe) for 10 min at room temperature, following which cells were incubated for another 30 min at 4°C after addition of a cocktail of metal conjugated antibodies targeting the surface antigens. Following two washes with CyFACS buffer, cells were fixed overnight using 4% formaldehyde made in PBS (VWR, Sweden). The broad extended panel of antibodies used for staining are listed in Supplementary Table S1. For acquisition by CyTOF (within 2 days after staining), cells were stained with DNA intercalator (0.125 μM Iridium-191/193 or MaxPar® Intercalator-Ir, Fluidigm) in 4% formaldehyde made in PBS for 20 min at room temperature. After multiple washes with CyFACS, PBS and milliQ water, cells were filtered through a 35-μm nylon mesh and diluted to 750 000 cells/ml. Cells were acquired at a rate of 300–500 cells/s using a super sampler (Victorian Airship, USA) connected to a CyTOF2 (Fluidigm) mass cytometer, CyTOF software version 6.0.626 with noise reduction, a lower convolution threshold of 200, event length limits of 10–150 pushes, a sigma value of 3 and a flow rate of 0.045 ml/min.

Antibodies and reagents

Purified antibodies for mass cytometry were obtained in carrier/protein-free buffer and then coupled to lanthanide metals using the MaxPar antibody conjugation kit (Fluidigm Inc.) as per the manufacturer's recommendations. Following the protein concentration determination by measurement of absorbance at 280 nm on a nanodrop, the metal-labeled antibodies were diluted in Candor PBS Antibody Stabilization solution (Candor Bioscience, Germany) for long-term storage at 4°C. Antibodies used are listed in Supplementary Table S1.

ProSeek data collection

Plasma protein data were generated using the proximity extension assay (ProSeek, Olink AB, Uppsala). Three panels (inflammation, metabolism and neuro-exploratory) were used to detect a range of biomarkers. Each panel kit provides a microtiter plate for measuring 92 protein biomarkers. Each well contains 96 pairs of DNA-labeled antibody probes. Samples were incubated in the presence of proximity antibody pairs tagged with DNA reporter molecules. When the antibody pair bounds to their corresponding antigens, the corresponding DNA tails form an amplicon by proximity extension, which can be quantified by high-throughput real-time PCR. The data were generated in a single batch (90 samples).

Whole blood mRNA-sequencing

Two milliliters of whole blood cryopreserved in PAXgene Blood RNA Tubes (cat.nr. 762165, Qiagen) were subjected to RNA isolation with QIAcube using PAXgene Blood RNA Kit (cat.nr. 762164, Qiagen). After elution, RNA quantity and quality (RIN value) were inspected with Qubit RNA HS Assay Kit (ThermoFisher, cat.nr. Q32855) and Agilent Technologies (cat.nr. 5067-1513), respectively.

Initial steps of RNA isolation consist of cell washing with ultrapure water followed by centrifugation to remove red blood cells. However, we could detect the presence of erythrocytes contents after washings (red pellet and high presence of mRNA from erythrocytes confirmed by qPCR). This interference of transcripts from red blood cells in extracted RNA from PAXgene tubes has been already described [55]. This non-complete depletion of erythrocytes during RNA extraction might hamper to perform reliable profiles of gene expression by masking relevant genes in the white blood cells content. In order to overcome that, we decided to use an approach developed by Krjutškov *et al.* [56] based on the blockage of alpha and beta-globin transcripts, two of the most highly expressed transcripts in erythrocytes. Briefly, ZNA-modified blocking oligos (lacking 3′-OH) annealing at 3′-end of mRNA molecules after RNA denaturation prevented the binding site of oligo-T primer, and therefore the generation of cDNA from these transcripts. Twenty nanograms of total RNA were used for blocking and cDNA synthesis with SMART-seq2 method [57]. After PCR, DNA was inspected with Qubit dsDNA HS Assay Kit (ThermoFisher, cat.nr. Q32854) and High Sensitivity DNA Analysis Kit (Agilent Technologies, cat.nr. 5067-4626). Nextera XT was then used to prepare DNA libraries for Illumina NovaSeq 6000 S2 (2 × 50 bp).

Oxygen consumption rate measurement

Seahorse XFe96 Analyzer (Seahorse Bioscience) was used to measure oxygen consumption rate (OCR) of ME-patient derived PBMCs. Frozen PBMCs were recovered in RPMI 1640 medium supplemented with 1% of penicillin–streptomycin solution and 10%

FBS for 4.5 h. One hour before the assay, the growth medium was replaced with Seahorse XF RPMI medium, and 3×10^5 PBMC per well were seeded with 40 µl assay medium in XF 96-well cell culture microplate coated with poly-D-lysine (Sigma). The plate was centrifuged at $200 \times g$ for 1 s with no brake, rotated 180° and centrifuged again for 1 s with no brake at $300 \times g$. After centrifugation, 140 µl of assay medium was added per well and the plate was left to stabilize in a 37°C non-CO_2 incubator. The wells were sequentially injected with 12.64 µM oligomycin (Sigma Aldrich 75351), 20 µM FCCP (Sigma Aldrich C2920), 5 µM rotenone (Sigma Aldrich R8875) together with 5 µM antimycin A (Sigma Aldrich A8674) and the OCR was measured for each well three times, every 3 min, before and after each injection. OCR was normalized to protein concentration following BCA assay conducted according to the manufacturer's instructions.

Mass cytometry preprocessing and gating

All FCS files were exported without any pre-processing from the CyTOF software and normalized using an in-house version of normalization software [58]. Debarcoding of each file was done using the MATLAB version of the single-cell debarcoder [59]. CellGrid, a supervised learning algorithm based on t-SNE implementation, was used to gate sub-cell populations [60].

ProSeek plasma protein data preprocessing

Olink's arbitrary unit is Normalized Protein eXpression which is Cq-values for each protein that are recalculated to a relative $\log_2$ scale. The data are normalized in order to minimize intra- and inter-assay variation, and the data from the three panels were merged to one dataset. If proteins were detected in less than 20% of all samples were removed and any missing values were set to the lowest detectable value for that protein. Due to the single batch experiment, no batch correction was necessary due to Olink's built-in quality control across panels, but batch effect check was performed indicating the same conclusion.

RNAseq data analysis

Quality control was provided by the National Genomics Infrastructure (NGI) at Science for Life Laboratory, Stockholm, Sweden. The first step after mRNA-sequencing was quantifying abundances of transcript sequences in FASTA format by generating abundance estimates for all samples using the Kallisto software [61]. Also, gene abundance estimates were performed by summing the transcript expression (TPM) values for the transcripts of the same gene. Since DESeq2 expects count data, from the Kallisto output the 'tximport' package was used to convert these estimates into read counts. DESeq2 was performed as a basis for differential gene expression analysis based on the negative binomial distribution [62]. Low gene counts (<100) were filtered out and variance stabilizing transformation was performed on the count data, as well as batch correction using the 'limma' package.

Analysis of variance in metabolomic data (Mito stress Seahorse assay)

Mixed-effects analysis using Sidak's multiple comparisons test over all timepoints (number of active treatments) was performed for maximal respiration and spare respiratory capacity results. Batch effect correction was performed beforehand using the 'limma' package, to then perform a mixed-effect model to account for paired sampling over treatment.

Automated cell classification

Grid is an in-house supervised algorithm based on the use of manually gated cell sub-populations as reference to train a classifier algorithm that can then classify similar cells quickly and accurately. The following populations were gated: B cells (IgD^+ memory B cells, IgD^- memory B cells, naïve B cells, transitional B cells and plasmablasts), CD4 T-cells (central memory CD4T, effector memory CD4T, naïve CD4T, naïve Tregs and memory Tregs), CD8 T-cells (activated CD8T, central memory CD8T, DP T-cells, effector memory CD8T and naïve CD8T), eosinophils, MAIT, monocytes (classical, non-classical and proinflammatory monocytes), natural killer (NK) cells ($CD56^{bright}$ NK and $CD56^{dim}$ NK), neutrophils, basophils, gdT ($CD161^+$ gdT and $CD161^-$ gdT) and pDC. These sub-populations were identified by phenotypic markers from the parameter selection.

Mixed-effects modeling

Complex mixed-effect models tend to result in singular fits; therefore, it is recommended to use a partially Bayesian method. The 'blme' package was applied on this data to produce maximum a posteriori estimates. This provided the ability to not only nest the variables, link individuals into sets of pre- and post-INMEST treatment, but also to account for sex, age as well as symptom scores and active treatments [63].

Multi-omics factor analysis

The input to MOFA is a set of matrices with dimensions (plasma protein expression, cell abundance and gene expression), the 'MOFAobject' was built using 'MultiAssayExperiment' object which was subsequently trained in R instead of Python through the 'reticulate' package. Prior to model training as the Gaussian noise model was used, methods like DESeq2 were performed on the mRNA-seq data for normalization and variance stabilization. All data sets were processed individually to remove any features resulting in zero or low variance before fitting the model. Convergence was assessed since MOFA is trained using variational Bayes which consists of the evidence lower bound (ELBO), therefore the change in ELBO (deltaELBO) was used and fit the convergence threshold which is considered to be between 1 and 10. The 'MOFAobject' was trained with 10 factors and a variance threshold of 0.01%. Multiple models under different initializations were run to make sure that factors were consistently found across trials for model selection.

Gene set enrichment analysis

GSEA was performed to investigate enriched gene sets in accordance to the number of active treatments [64]. These groups of genes were derived from the mixed-effect modeling and then 'gseGO' was used for GSEA looking at GO terms for Biological Processes with *P*-values calculated from mixed-effect modeling.

Disease tolerance networks

Disease tolerance networks were built by finding key regulators for query genes using Han *et al.* from TRRUST v2 [45]. Edge and node dataframes were built from information acquired from TRRUST v2 with the addition of calculated $\log_2$(treated/baseline) for color gradient. Node sizes were based on the number of edges, the larger the node the more the edges. These were used to build the networks with 'visNetwork()'.

Supplementary data

Data and materials availability

FCS files from Mass Cytometry experiments are available at: http://flowrepository.org/id/FR-FCM-Z2F2. All scripts for reproduction of each figure of the manuscript are available through our dedicated GitHub repository: https://github.com/Brodinlab/ME-CFS_study.git. All correspondence and material requests should be addressed to P.B., petter.brodin@ki.se.

Authors' contributions

Funding

Conflict of interest statement

J.-E.J. is a co-founder and shareholder of Abilion Medical Systems AB. P.B., T.L., A.O. and J.M. are founders of Cytodelics AB, a company commercializing reagents for blood sample preservation used in this study.

Acknowledgements

References

1. Komaroff AL. Advances in understanding the pathophysiology of chronic fatigue syndrome. *JAMA* 2019;**322**:499–500.
2. Clayton EW. Beyond myalgic encephalomyelitis/chronic fatigue syndrome: An IOM report on redefining an illness. *JAMA* 2015;**313**:1101–2.
3. Bested AC, Marshall LM. Review of myalgic encephalomyelitis/chronic fatigue syndrome: An evidence-based approach to diagnosis and management by clinicians. *Rev Environ Health* 2015;**30**:223–49.
4. Blundell S, Ray KK, Buckland M *et al.* Chronic fatigue syndrome and circulating cytokines: A systematic review. *Brain Behav Immun* 2015;**50**:186–95.
5. Montoya JG, Holmes TH, Anderson JN *et al.* Cytokine signature associated with disease severity in chronic fatigue syndrome patients. *Proc Natl Acad Sci USA* 2017;**114**:E7150–8.
6. Karhan E, Gunter CL, Ravanmehr V *et al.* Perturbation of effector and regulatory T cell subsets in myalgic encephalomyelitis/chronic fatigue syndrome (ME/CFS). Biorxiv 2019.12.23.887505, 2019.
7. Brodin P. The biology of the cell- insights from mass cytometry. *The FEBS journal* 2019;286(8):1514–1522.
8. Lundberg M, Eriksson A, Tran B *et al.* Homogeneous antibody-based proximity extension assays provide sensitive and specific detection of low-abundant proteins in human blood. *Nucleic Acids Res* 2011;**39**:e102.
9. Gomes T, Teichmann SA, Talavera-López C. Immunology driven by large-scale single-cell sequencing. *Trends Immunol* 2019;**40**:1011–21.
10. Davis MM, Brodin P. Rebooting human immunology. *Annu Rev Immunol* 2018;**36**:1–22.
11. Brodin P, Davis MM. Human immune system variation. *Nat Rev Immunol* 2016;**17**:21–9.
12. Brodin P, Jojic V, Gao T *et al.* Variation in the human immune system is largely driven by non-heritable influences. *Cell* 2015;**160**:37–47.
13. Tsang JS. Utilizing population variation, vaccination, and systems biology to study human immunology. *Trends Immunol* 2015;**36**:479–93.
14. Lakshmikanth T, Olin A, Chen Y *et al.* Mass cytometry and topological data analysis reveal immune parameters associated with complications after allogeneic stem cell transplantation. *Cell Rep* 2017;**20**:2238–50.
15. Chowdhury RR, Vallania F, Yang Q *et al.* A multi-cohort study of the immune factors associated with *M. tuberculosis* infection outcomes. *Nature* 2018;**560**:644–8.
16. Krieg C, Nowicka M, Guglietta S *et al.* High-dimensional single-cell analysis predicts response to anti-PD-1 immunotherapy. *Nat Med* 2018;**24**:144–53. https://10.1038/nm.4466.
17. Tracey KJ. The inflammatory reflex. *Nature* 2002;**420**:853–9.
18. VanElzakker MB. Chronic fatigue syndrome from vagus nerve infection: A psychoneuroimmunological hypothesis. *Med Hypotheses* 2013;**81**:414–23.
19. Rowe PC, Marden CL, Heinlein S *et al.* Improvement of severe myalgic encephalomyelitis/chronic fatigue syndrome symptoms following surgical treatment of cervical spinal stenosis. *J Transl Med* 2018;**16**:21.
20. Proal A, Marshall T. Myalgic encephalomyelitis/chronic fatigue syndrome in the era of the human microbiome: Persistent pathogens drive chronic symptoms by interfering with host metabolism, *gene expression, and immunity. Front Pediatr* 2018;**6**:373.
21. Addorisio ME, Imperato GH, Vos AF de *et al.* Investigational treatment of rheumatoid arthritis with a vibrotactile device applied to the external ear. *Bioelectron Med* 2019;**5**:4.
22. Lerman I, Hauger R, Sorkin L *et al.* Noninvasive transcutaneous vagus nerve stimulation decreases whole blood culture-derived cytokines and chemokines: A randomized, blinded, healthy control pilot trial. *Neuromodulation Technol Neural Interface* 2016;**19**:283–90.
23. Jerling M, Cygankiewicz I, Al-Tawil N *et al.* Effects of intranasal kinetic oscillation stimulation on heart rate variability. *Ann Noninvasive Electrordiol* 2018;**23**:e12474. doi:10.1111/anec.12474

24. Li T-Q, Wang Y, Fukunaga M. Detection of BOLD response in the limbic system to non-invasive stimulation of autonomic nervous system with SMS at 7T. 2018. https://cds.ismrm.org/protected/18MProceedings/PDFfiles/4537.html

25. Li T-Q, Wang Y, Hallin R *et al.* Resting-state fMRI study of acute migraine treatment with kinetic oscillation stimulation in nasal cavity. *Neuroimage Clin* 2016;**12**:451–9.

26. Juto J-E, Axelsson M. Kinetic oscillation stimulation as treatment of non-allergic rhinitis: An RCT study. *Acta Otolaryngol* 2014;**134**:506–12.

27. Möller M, Mehnert J, Schroeder CF *et al.* Noninvasive vagus nerve stimulation and the trigeminal autonomic reflex: An fMRI study. *Neurology* 2020;**94**:10.1212/WNL.0000000000008865.

28. Möller M, Schroeder CF, May A. Vagus nerve stimulation modulates the cranial trigeminal autonomic reflex. *Ann Neurol* 2018;**84**:886–92.

29. Rainen L, Oelmueller U, Jurgensen S *et al.* Stabilization of mRNA expression in whole blood samples. *Clin Chem* 2002;**48**:1883–90.

30. Krupp LB, LaRocca NG, Muir-Nash J *et al.* The fatigue severity scale. *Arch Neurol* 1989;**46**:1121.

31. Jonsjö MA, Wicksell RK, Holmström L *et al.* Identifying symptom subgroups in patients with ME/CFS—relationships to functioning and quality of life. *Fatigue Biomed Heal Behav* 2017;**5**:33–42.

32. Argelaguet R, Velten B, Arnol D *et al.* Multi-omics factor analysis—a framework for unsupervised integration of multi-omics data sets. *Mol Syst Biol* 2018;**14**:e8124.

33. Cooper MA, Fehniger TA, Turner SC *et al.* Human natural killer cells: A unique innate immunoregulatory role for the CD56(bright) subset. *Blood* 2001;**97**:3146–51.

34. Hotson AN, Gopinath S, Nicolau M *et al.* Coordinate actions of innate immune responses oppose those of the adaptive immune system during *Salmonella* infection of mice. *Sci Signal* 2016;**9**:ra4.

35. VanElzakker MB, Brumfield SA, Mejia PSL. Neuroinflammation and cytokines in myalgic encephalomyelitis/chronic fatigue syndrome (ME/CFS): A critical review of research methods. *Front Neurol* 2019;**9**:1033.

36. Whibley N, Tucci A, Powrie F. Regulatory T cell adaptation in the intestine and skin. *Nat Immunol* 2019;**20**:386–96.

37. Salloum N, Hussein HM, Jammaz R *et al.* Epstein–Barr virus DNA modulates regulatory T-cell programming in addition to enhancing interleukin-17A production via Toll-like receptor 9. *PLoS ONE* 2018;**13**:e0200546.

38. Brodin P, Duffy D, Quintana-Murci L. A call for blood—in human immunology. *Immunity* 2019;**50**:1335–6.

39. Huang C-C, Chiu T-Y, Lee T-Y *et al.* Soluble α-synuclein facilitates priming and fusion by releasing Ca^{2+} from thapsigargin-sensitive Ca^{2+} pool in PC12 cells. *J Cell Sci* 2018;**131**:jcs.213017.

40. Esfandyarpour R, Kashi A, Nemat-Gorgani M *et al.* A nanoelectronics-blood-based diagnostic biomarker for myalgic encephalomyelitis/chronic fatigue syndrome (ME/CFS). *Proc Natl Acad Sci USA* 2019;**116**:201901274.

41. Armstrong CW, McGregor NR, Lewis DP *et al.* Metabolic profiling reveals anomalous energy metabolism and oxidative stress pathways in chronic fatigue syndrome patients. *Metabolomics* 2015;**11**:1626–39.

42. Matschinsky FM, Wilson DF. The central role of glucokinase in glucose homeostasis: A perspective 50 years after demonstrating the presence of the enzyme in islets of langerhans. *Front Physiol* 2019;**10**:148.

43. Holden S, Maksoud R, Eaton-Fitch N *et al.* A systematic review of mitochondrial abnormalities in myalgic encephalomyelitis/chronic fatigue syndrome/systemic exertion intolerance disease. *J Transl Med* 2020;**18**:290.

44. Martins R, Carlos AR, Braza F *et al.* Disease tolerance as an inherent component of immunity. *Annu Rev Immunol* 2019;**37**:405–37.

45. Han H, Cho J-W, Lee S *et al.* TRRUST v2: An expanded reference database of human and mouse transcriptional regulatory interactions. *Nucleic Acids Res* 2017;**46**:D380–6.

46. Saha AK, Schmidt BR, Wilhelmy J *et al.* Red blood cell deformability is diminished in patients with chronic fatigue syndrome. *Clin Hemorheol Microcirc* 2019;**71**:113–6.

47. Dumitru C, Kabat AM, Maloy KJ. Metabolic adaptations of CD^{4+} T cells in inflammatory disease. *Front Immunol* 2018;**9**:540.

48. Morris G, Anderson G, Maes M. Hypothalamic–pituitary–adrenal hypofunction in myalgic encephalomyelitis (ME)/chronic fatigue syndrome (CFS) as a consequence of activated immune-inflammatory and oxidative and nitrosative pathways. *Mol Neurobiol* 2017;**54**:6806–19.

49. Kashi AA, Davis RW, Phair RD. The IDO metabolic trap hypothesis for the etiology of ME/CFS. *Diagnostics* 2019;**9**:82.

50. Bessede A, Gargaro M, Pallotta MT *et al.* Aryl hydrocarbon receptor control of a disease tolerance defence pathway. *Nature* 2014;**511**:184–90.

51. Soares MP. "Nuts and bolts" of disease tolerance. *Immunity* 2014;**41**:176–8.

52. Preez SD, Corbitt M, Cabanas H *et al.* A systematic review of enteric dysbiosis in chronic fatigue syndrome/myalgic encephalomyelitis. *Syst Rev* 2018;**7**:241.

53. Jason L, Evans JM, Brown M *et al.* Fatigue scales and chronic fatigue syndrome: Issues of sensitivity and specificity. *Disabil Stud Q* 2011;**31**:1375. doi:10.18061/dsq.v31i1.1375

54. Carruthers BM, Sande MI van de, Meirleir KLD *et al.* Myalgic encephalomyelitis: International consensus criteria. *J Intern Med* 2011;**270**:327–38.

55. Joehanes R, Johnson AD, Barb JJ *et al.* Gene expression analysis of whole blood, peripheral blood mononuclear cells, and lymphoblastoid cell lines from the Framingham Heart Study. *Physiol Genomics* 2011;**44**:59–75.

56. Krjutškov K, Koel M, Roost AM *et al.* Globin mRNA reduction for whole-blood transcriptome sequencing. *Sci Rep* 2016;**6**:31584.

57. Picelli S, Björklund ÅK, Faridani OR *et al.* Smart-seq2 for sensitive full-length transcriptome profiling in single cells. *Nat Methods* 2013;**10**:1096–8.

58. Finck R, Simonds EF, Jager A *et al.* Normalization of mass cytometry data with bead standards. *Cytom Part A* 2013;**83A**:483–94.

59. Zunder ER, Finck R, Behbehani GK *et al.* Palladium-based mass tag cell barcoding with a doublet-filtering scheme and single-cell deconvolution algorithm. *Nat Protoc* 2015;**10**:316–33.

60. Chen Y, Lakshmikanth T, Mikes J *et al.* Single-cell classification using learned cell phenotypes. *Biorxiv* 2020:2020.07.22.216002.

61. Bray NL, Pimentel H, Melsted P *et al.* Near-optimal probabilistic RNA-seq quantification. *Nat Biotechnol* 2016;**34**:525–7.

62. Love MI, Huber W, Anders S. Moderated estimation of fold change and dispersion for RNA-seq data with DESeq2. *Genome Biol* 2014;**15**:550.

63. Chung Y, Rabe-Hesketh S, Dorie V *et al.* A nondegenerate penalized likelihood estimator for variance parameters in multilevel models. *Psychometrika* 2013;**78**:685–709.

64. Subramanian A, Tamayo P, Mootha VK *et al.* Gene set enrichment analysis: A knowledge-based approach for interpreting genome-wide expression profiles. *Proc Natl Acad Sci USA* 2005;**102**:15545–50.